Supplementary Information

Glutamine based PET imaging facilitates enhanced metabolic evaluation of gliomas *in vivo*.

Authors: Sriram Venneti*[1], Mark P. Dunphy*[2], Hanwen Zhang*[3], Kenneth L. Pitter[1], Patrick Zanzonico[4], Carl Campos[5], Sean D. Carlin[6], Gaspare La Rocca, Serge Lyashchenko[7], Karl Ploessl[8], Daniel Rohle[1,5], Antonio M. Omuro[9], Justin R. Cross[11], Cameron W. Brennan[5,10], Wolfgang A. Weber[2,3], Eric C. Holland[1,9,10,§], Ingo K. Mellinghoff[5,9], Hank F. Kung[8], Jason S. Lewis[#3,6,7] and Craig B. Thompson[#1,5]

* These authors contributed equally to this study.

Table of Contents

Materials and Methods

Cell culture

Previously well-characterized cell lines were obtained from the MSKCC brain tumor center (*11*). All cell lines were negative for mycoplasma. TS543 (PDGFRA amplification and PTEN -/-), TS603 (bearing endogenous IDH1 R132H mutation), U87-MG (PTEN-/-) and TS598 (EGFR amplification) were cultured in 10 cm petri dishes under neurosphere conditions. Briefly, cells were cultured in serum free stem cell media (neurobasal media supplemented with B27, epidermal growth factor (20 ng/mL), fibroblast growth factor (10 ng/mL) and heparin (2 μg/mL). SF188 glioma cell lines were cultured in Dulbecco's Modified Eagle Medium with 10% fetal calf serum and 1% Penicillin Streptomycin (*27*).

Metabolism experiments

Metabolic tracing experiments were conducted as previously described(*27*). Cells were incubated with glutamine-free neurobasal media supplemented with 2 mM [U-^{13}C]-glutamine or glucose-free neurobasal media supplemented with 20 mM [U-^{13}C]-glucose. After 24 hours, cells were collected by centrifugation at 1200 rpm for 5 minutes, washed in PBS and rapidly quenched with 80% methanol (-80°C) containing a M+5 internal standard of *D*(−)-2HG with five deuterium atoms (D-2-hydroxyglutaric-2,3,3,4,4-d_5 acid, D-2HG). Following incubation at -80°C for 24 h, cell extracts were harvested and proteins were pelleted out by centrifugation at 14,000 *g* for 15 min. Protein content in pellets

was measured using the Pierce BCA protein assay kit (Thermoscientific) and normalized to ^{13}C isotope labeled values for each metabolite. Supernatants were dried in an evaporator (Genevac EZ-2) under nitrogen gas, dissolved in methoxamine/pyridine and 1:1 acetonitrile:*N*-methyl-*N*-tertbutyldimethylsilyltrifluoroacetamide (MTBSTFA; Regis), and heated at 70°C for 80 min to derivatize metabolites. Gas chromatography mass spectroscopy (GC-MS) was conducted as previously described(*27*). Enrichment of ^{13}C isotope was evaluated by measuring the abundance for the following ions: *m/z* 245-254 for fumarate, *m/z* 335-348 for malate, *m/z* 334-346 for aspartate, *m/z* 465-482 for citrate, *m/z* 174-$^{18}0$ for pyruvate, *m/z* 219-227 for lactate, *m/z* 363-377 for glutamate, *m/z* 362-376 for glutamine and *m/z 349-362* for D-2HG. D-2HG levels were determined by normalizing to protein content as well as the internal D-2HG standard.

The half-life of ^{18}F is ~110 minutes, which limits metabolic analysis on a GC-MS. To overcome this limitation we labeled glutamine with stable fluorine isotope ^{19}F (^{19}F-FGln, identical to ^{18}F-FGln, except ^{18}F is replaced by ^{19}F). Glioma cell lines were incubated with 2 mM ^{19}F-FGln or [U-^{13}C]-glutamine for 0.5, 1 and 2 hours. Pure ^{19}F-FGln (*m/z* 365) and ^{19}F-labeled glutamate (^{19}F-FGlu, *m/z* 366) were run as standards. ^{19}F-labeled glutamate or glutamine was extracted in reference to the standards and ^{13}C-labeled glutamate or glutamine was extracted as described above.

IDH1 knockdown and pharmacologic inhibition of mIDH1

Knockdown of total IDH1 was performed using shRNA as previously described(*11*). Briefly, lentiviruses bearing either the pTRIPz empty vector

(Thermo scientific) or IDH1 sh484 (targeting the coding sequence) were generated using 293T cells co-transfected with pTRIPz vectors and trans-lentiviral shRNA packaging kit (Addgene) (*11*). TS603 cells were infected with supernatant from 293T cells containing viral particles. Pharmacological inhibition of IDH1m was achieved by treating cells with the IDH1m inhibitor IDH35 (1500 nM, Xcessbio Pharma) for 48hours as previously described (*11*).

Western blotting

Cells were lysed with RIPA buffer containing protease inhibitor cocktail (Roche) and phosphatase inhibitor cocktails 2 and 3 (Sigma). Lysates were centrifuged at 14,000*g* for 20 min at 4°C and supernatants were harvested. Protein concentrations in supernatants were detected with the BCA Protein Assay (Pierce). Lysates were separated by SDS-PAGE on Novex 4-12% Bis-Tris gels (Invitrogen), transferred to nitrocellulose membranes, and blocked in 5% nonfat milk in PBS containing 0.2% Tween-20. Membranes were probed with mouse monoclonal anti-IDH1 R132H (DIA H09, Dianova; 1:500) or rabbit polyclonal anti-SLC1A5 (ABN73, Milipore; 1:1000) or mouse monoclonal anti-β-actin (sc-47778, Santa Cruz; 1:10,000) or anti-β-tubulin (sc-9105, Santa Cruz; 1:10,000). Detection was performed with horseradish-peroxidase-conjugated anti-mouse antibody (NA931V, GE Healthcare; 1:10,000).

Animal models of neuroinflammation

Mouse models of neuroinflammation were generated by injecting 4-6 week-old, male or female C57BL6 mice with lipopolysaccharide (5 μg) or a mixture of

interferon-γ/ interleukin-4 (5 international units each) in the right frontal cortex (same stereotactic coordinates as tumor injection). Animals were randomly divided into groups that were either injected with LPS or interferon-γ/ interleukin-4. Individuals performing stereotactic injections were blinded to the experimental design. Neuroinflammation was confirmed by histologic evaluation for activated microglia/ macrophages by immunostaining for IBA1 and evaluating reactive astrogliosis by immunostaining for GFAP as detailed in the immunohistochemitry section. Neuroinflammation peaks at four days post injection when mice were imaged.

Animal model of disrupted BBB

Increased permeability of the BBB was achieved in mice as previously described (*15*). NECA [1-(6-amino-9H-purin-9-yl)-1-deoxy-N-ethyl-β-D-ribofuranuronamide] (Tocris Bioscience) was resuspended in DMSO then diluted in PBS to a concentration of 30 μM stock solution (for vehicle controls, DMSO was diluted in PBS to achieve the same concentration). 10 KDa dextrans labeled with FITC was resuspended in PBS at a concentration of 50 mg/ml. Either NECA (final concentration of 0.08 mg/kg (*15*)) or vehicle and 1.0 mg of dextran in PBS was injected retro-orbitally into the intravenous space. Mice were imaged with PET 5 hours post injection at the peak of BBB permeability(*15*). After imaging, mice were anesthetized and perfused with cold PBS. The brain was rapidly extracted, weighed and homogenized in Tris-Cl (50mM, pH7.6,100 μL per 100 mg brain) with a Dounce homogenizer and centrifuged at 16 *g* for 30 min. Supernatants were then mixed with an equal volume of absolute methanol and were centrifuged again at 16 *g* for 30 min. Supernatants were transferred to a Corning

Costar 96 well black polystyrene assay plate (clear bottom) and were read on a Fluorimetric 96 plate reader with dextran in 50% Tris-Cl/50% absolute methanol (v/v) as positive controls and Tris-Cl/50% absolute methanol (v/v) as negative controls.

Chemo/radiation therapy in animal models

RCAS-PDGF, PTEN -/- animals were treated with chemotherapy and radiation therapy for 5 days similar to previously published protocols(*17*). The individual administering treatment was blinded to the experimental design. Animals were treated with the chemotherapeutic agent Temozolomide (50mg/mL, one hour prior to irradiation) by oral gavage to lessen the risk of acute organ toxicity or extravasation associated with intravenous injection. Animals were irradiated using an X-RAD 320 machine (Precision X-Ray) at 155 cGy/min. Only the head of the animal was irradiated; the body was protected with lead jig to minimize radiation toxicity to normal tissues. Animals were imaged after a 24-hour recovery period. For PET and MRI imaging, the same animal (RCAS-PDGF, PTEN -/-) was compared before and after imaging. Further, RCAS-PDGF, PTEN -/- animals imaged before treatment were compared with animal models of neuroinflammation and animals with disrupted blood brain barrier.

Small animal magnetic resonance imaging (MRI)

MRI was acquired prior to PET imaging. Mice were anesthetized (1-2% isoflurane gas) and imaged on a 4.7-Tesla Biospec scanner with a 12-cm gradient coil, operating at 200 MHz (400 mT/m ID; Bruker Biospin MRI GmbH).

Mice were positioned in the scanner by acquiring T2-weighted scout images along 3 orthogonal orientations and the body temperature was maintained using a heated air system (Air-Therm Heater, World Precision Instruments, Sarasota, FL). T2-weighted mouse cranial images (slice thickness of 0.8 mm and a field of view of 30×34 mm with a spatial resolution of 117×133 μm) were acquired using fast spin-echo sequences (rapid acquisition with relaxation enhancement [RARE]) with the following acquisition parameters: repetition time, 4.5 s; echo time, 40 ms; RARE factor, 8; and acquisition time, 20 min. The individual performing the MRIs was blinded to the experimental design.

Biodistribution Studies

Mice injected with ^{18}F-FGln intravenously in the tail were euthanized by CO_2 gas asphyxiation at 15, 30, 60 and 120 min (n=5 each time point) after injection. Various tissues were rapidly removed, rinsed in PBS, weighed and placed in tubes to measure activity on a γ-counter (Perkin Elmer) using ^{18}F-FGln standards to determine the total number of counts per minute. In parallel experiments, 60 microcuries of ^{18}F-FGln was injected with or without cold excess ^{19}F-FGln (150 mM) in a final volume of 150 μL. Tissue uptake of ^{18}F-FGln was measured as percentage of injected dose per gram of tissue (%ID/g) after correcting for background and decay. ^{18}F-Sodium fluoride was used as a control in separate experiments to compare free fluoride uptake in bone and various organs with ^{18}F-FGln uptake.

Autoradiography

Ex-vivo autoradiography was performed on frozen sections (10 μM thick, cut on HM 500 M cryostat at -20^{o}C) of the brain rapidly removed after 30 min post radiotracer injection. A FujiFilm BAS-^{18}00 II device (Fuji Photo Film) was used to create 16-bit grayscale digital images (50 μM pixel resolution). The individual performing autoradiography was blinded to the experimental design.

SLC1A5 knockdown and uptake studies

SLC1A5 was knocked down in SF188 glioma cell lines with four different siRNAs. Scrambled siRNA was used as control. In brief, siRNAs were added to Opti-MEM Reduced Serum Medium (31985070, Life Technologies) containing Lipofectamine RNAiMAX (13778075, Life Technologies). Cells were lysed 72 hours after transfection and protein extracts were probed with an antibody specific to SLC1A5 (see western blotting). Decreased glutamine uptake was confirmed using YSI 7100 MBS (YSI Life Science). The SLC1A5 inhibitor γ-L-glutamyl-p-nitroanilide (GPNA, 5mM, 0210066301, Sigma) was used at concentrations previously shown to inhibit glutamine uptake (*19*). Glutamine cell uptake studies were performed by plating cells at a density of 2.5 X 10^5 cells in complete media as previously described (*8*) (*19*). Cells were washed three times with PBS after aspirating media. ^{18}F-FGln (0.4 μCi/well) dissolved in PBS was added to each well and incubated for 1 hour at 37 ^{0}C, following which the cells were washed with ice cold PBS and lysed with 350 μL of sodium hydroxide.

Specific activity in lysates was determined using a gamma counter and normalized to protein content.

Human subjects

In vivo PET imaging of six human glioma subjects was conducted as part of a Phase I, IRB and FDA approved study. The clinical histories of the patients are presented below.

Patient #1: A 54-year old male diagnosed with Oligoastrocytoma, WHO grade II. Molecular analyses of tumor material revealed methylation at the MGMT promoter region. The tumor did not bear IDH mutations or 1p-19q co-deletions. The patient was treated with the immunostimulant Poly ICLC (Toll like receptor 3 activator composed of carboxymethylcellulose, polyinosinic-polycytidylic acid, and poly-L-lysine double-stranded RNA). Poly ICLC treatment was stopped two months prior to imaging. Serial gadolinium enhanced- MRI showed minimal increase in tumor volume without contrast enhancement. The patient remained clinically stable since diagnosis till the time of the study.

Patient #2: A 37-year old female diagnosed with Oligoastrocytoma, WHO grade II. Molecular analyses of tumor material revealed IDH1 R132H mutation. No 1p-19q co-deletions were detected. The patient was treated with Temozolomide which was stopped 11 months prior to the current study. The patient remained clinically stable since diagnosis till the time of the study (period of 5.6 years follow up period). Serial gadolinium enhanced- MRI showed no significant

change in tumor volume or contrast enhancement during the period of follow up till the time of the study.

Patient #3: A 71-year old female diagnosed with an Astrocytoma, WHO grade II. Molecular analyses of tumor material revealed IDH1 R132H mutation and methylation at the MGMT promoter region. No 1p-19q co-deletions were detected. The patient was followed up for a period of 1.5 years prior to the current study and remained clinically stable with no significant change in tumor volume or contrast enhancement till the time of the study.

Patient #4: A 53-year old female was diagnosed with an Astrocytoma, WHO grade II in the left parietal lobe. The patient was treated with chemoradiation therapy that was stopped 14 months prior to the current study. Prior to imaging studies the patient showed 3 lesions, the first lesion remained stable during the follow up period. The other two lesions showed rapid increase in size with contrast enhancement during a four month follow up period. One of the two rapidly growing lesions was biopsied after PET imaging and was diagnosed as high-grade Anaplastic Astrocytoma. Molecular analysis showed EGFR amplification and EGFR VIII mutations. The tumor was IDH wild type.

Patient #5: A 42-year old male diagnosed with Oligodendroglioma. The tumor was graded as WHO grade II but the Neuropathologist at the time noted that tumor showed “regionally elevated Ki-67 labeling activity indicating a possible higher biologic potential that that associated with the usual grade II lesion”. Molecular analyses of tumor material revealed IDH1 R132H mutation and 1p-19q

co-deletion. The patient had two lesions, one remained clinically stable without increase in size or contrast enhancement over the follow up of 4.5 years while the second increased in size without contrast enhancement during the past year.

Patient #6: A 57-year old male was diagnosed with glioblastoma, WHO grade IV. Molecular analyses of tumor showed no MGMT promoter methylation or IDH mutations. The patient was treated with chemoradiation therapy that was stopped 3 months prior to the current study. Over a follow up period of 0.8 years, MRI showed a lesion increasing in size with contrast enhancement prior to the study.

PET imaging in human glioma patients

Demographic data of patients imaged are given in **table S1**. Physical and laboratory examinations were obtained within 2-weeks before study participation, including complete blood count and liver and renal function tests. A study physician monitored patients closely for toxicity. Subjects fasted at least 8 hours prior to tracer-injection until completion of the blood sampling and imaging. An intravenous catheter was placed in each upper extremity. One catheter was used for tracer administration and the other catheter for blood sampling. Trial eligibility criteria included (1) histologically-confirmed malignancy, (2) measurable or evaluable disease by standard tumor imaging criteria, (3) age between 21-90 years and (4) serum renal and hepatic function test values within allowed range (less than 1.5-2.5 fold greater than lab-specific upper limit of normal). Exclusion criteria included (1) pregnancy or breast-feeding, (2) impaired renal or liver function tests and (3) acute major illness. We compared ^{18}F-FGln uptake in 3

patients with stable disease with 3 patients showing glioma progression in a non-blinded manner.

MRI protocol

MRI scans were obtained as part of routine clinical care using hardware and standard data acquisition and processing methods. MRI was obtained using a 1.5 T magnet (Signa HDxt, GE Healthcare). Images were acquired using 5-mm slice thickness with no interslice gap (repetition time (TR) / echo time (TE) = 500/10 msec, matrix 256×256). Gadopentetate dimeglumine (Magnevist, HealthCare Pharmaceuticals Inc.) was injected though a peripheral angiocatheter at a standard dose (0.2 mL/kg body weight, 40 mL, 2 cc/sec).

^{18}F-FDG PET-CT protocol

^{18}F-FDG PET-CT brain scans were obtained in 5 patients (patients #1-3,5 and 6) as part of routine clinical care using PET-CT camera systems and clinical standard data acquisition and processing methods. In brief, PET/CT scans were performed using a PET-CT scanner (Discovery DSTE or Discovery 690, GE Healthcare). Patients fasted at least 6 hours for the study. Plasma glucose was assayed immediately prior to ^{18}F-FDG injection, found to be less than 200 mg/dL in all cases. No patients were diabetic, though diabetes was not an exclusion criterion. Each patient underwent PET/CT scanning at 62 ± 4 minutes after tracer injection with 390 ± 37 MBq ^{18}F-FDG. Patients were scanned in supine position on scanner bed, with upper extremities lowered at sides. After scout X-ray, head CT was acquired with 120 kvp; 150 mA; pitch of 1.75:1; reconstructed

slice thickness of 3.75 mm; 0.8 s per rotation. CT data were reconstructed in a 512 × 512 matrix using a filtered back-projection algorithm. PET emission scans were acquired of the entire brain, 5 minutes per bed position in 3-D mode. PET emission data were reconstructed using an ordered subset expectation maximization iterative algorithm. Emission data were corrected for detector inhomogeneity, scatter, attenuation, deadtime, and decay. PET emission data were reconstructed to a 256 x 256 matrix over a 30 cm field of view. PET data was analyzed using HERMES workstation. ^{18}F-FGln PET-CT, ^{18}F-FDG brain PET-CT, and brain MRI clinical scans were displayed for analytic comparison using an integrated GE PACS AW Suite workstation (GE Healthcare). ^{18}F-FDG PET-CT scans were obtained 7,1, and 6 days prior to ^{18}F-FGln PET-CT in patients #1, 2, and 6, respectively; and 1.9 and 1.8 years prior, in patients #3 and #5, respectively). Patient #4 had no ^{18}F-FDG PET-CT scan. A limitation of this study is that ^{18}F-FDG PET scans were obtained from patients #3 and #5, ~2 years prior to ^{18}F-FGln imaging.

Tracer-biodistribution was quantified by software-based measurements of organ activity concentrations derived from PET imagery, using standard manually-placed digital volumes-of-interest (VOI). Organ activity concentrations were expressed as the organ VOI average standard uptake value (SUV), normalizing tissue activity concentrations to patient body mass. The SUV was calculated by the standard formula [SUVbw = C(t) / (D/W)]; SUVbw is the calculated tracer concentration in the organ of interest; C(t) is the measured activity concentration in the organ of interest, in units of Bq per mL of tissue; D is the amount of administered activity, in Bq; and W is the patient body mass, in grams.

Blood sampling and analysis

Plasma clearance of radioactivity and tracer metabolism were assayed by serial blood draws. Blood samples were collected ~5, 10, 20, 30, and 150 min after tracer injection, recording exact sampling times. Catheters were saline flushed between blood samplings, and an initial blood sample was discarded immediately prior to each blood collection. ~5 mL blood samples were collected in heparinized tubes and kept on wet ice until radioassay. From each sample, aliquots of blood were separated for well-counting and radioHPLC-based metabolite analysis. Activity in whole blood and plasma was radioassayed by well counter (1480 WIZARD® 3" Automatic Gamma Counter, PerkinElmer), after separating blood and plasma by centrifuge. Well counting obtained a minimum of 10,000 counts per specimen; correcting for background activity and radioactive-decay from time of tracer-injection. An ^{18}F standard was assayed on the well counter to obtain a calibration factor for converting sample scintillation counts to becquerels of activity. Dividing sample activity by the sample volume and intravenously-administered radioactivity quantified the sample activity in terms of fraction-of-injected-dose per mL (ID/mL). The ID/mL value was multiplied by the patient body weight (g) to convert to standard uptake values (SUV) for comparison with tumor SUV values measured by PET. For radioHPLC of blood aliquots, serum proteins were precipitated with ethanol (v/v=1/1), then the samples were centrifuged for 10 min at 9,000 rpm. The supernatant was removed by filtration with 0.22 um filter, and then the sample was diluted with water (v/v=1/5). One mL of the solution was characterized with an analytical chiral HPLC (Chirex 3126 (d)-penicillamine; mobile phase: 1 mM $CuSO_4$ solution; flow rate: 1 mL/min; room

temperature). Elution fractions were collected every 30 seconds and measured on the gamma counter (WIZARD™ 3" 1480 γ-counter, PerkinElmer).

Human glioma samples

Human glioma samples (n=64) and 8 normal brain samples were obtained from the University of Pennsylvania after approval from the institutional review board and after removal of all patient identifiers. Samples were assayed using immunohistochemistry in a blinded manner. The cohort consisted of a total of 8 normal brain and 64 glioma samples (7 WHO grade II oligodendrogliomas, 11 grade III anaplastic oligodendrogliomas, 13 grade III anaplastic astrocytomas, 33 grade IV glioblastomas). Sections were also obtained from ^{18}F-FGln imaged patients #2-6 (material was not available from patient #1). A neuropathologist evaluated all cases in a blinded manner. The TCGA Data Portal was used to analyze data for SLC1A5 expression in GBM (http://cancergenome.nih.gov, accessed on April 04, 2014). mRNA expression z-scores (with a z-score threshold ± 2) for SLC1A5 were obtained for the proneural G-CIMP+ve, proneural G-CIMP-ve, classical, mesenchymal and neural GBM subgroups.

Immunohistochemistry

Immunostaining was performed using the Discovery XT processor (Ventana Medical Systems). Tissue sections were blocked for 30 min in 10% normal goat serum in 2% BSA in PBS. Sections were incubated for 5 h with one of the following antibodies: (1) mouse monoclonal anti-IDH1 R132H (DIA H09, Dianova; 1:30), (2) rabbit polyclonal anti-IBA1 (#5076, Abcam; 0.5 μg/mL), (3) rabbit

polyclonal anti-olig-2 (#81093**,** Abcam; 2μg/mL), (4) rabbit monoclonal anti-PDGFRA (#3174; Cell signaling; 1:500 dilution), (5) rabbit polyclonal anti-GFAP (#Z0334; DAKO; 1μg/ml dilution), (6) rabbit polyclonal anti-CD3, (#A0452; DAKO; 1.2μg/ml dilution), (7) rat monoclonal anti-CD31 (#DIA-310; DIANOVA; 1μg/ml dilution), (8) rabbit polyclonal anti-SLC1A5 (#HPA035240; SIGMA; 0.5 μg/ml dilution), and (9) rabbit polyclonal anti-collagen IV (# 2150-1470, Serotec; 1μg/ml). Tissue sections were then incubated for 60 min with biotinylated goat anti-rabbit IgG (Vector labs, PK6101) at 1:200 dilution. Blocker D, Streptavidin-HRP and DAB detection kit (Ventana Medical Systems) were used according to the manufacturer instructions.

For automated scoring, each slide was scanned using a Pannoramic Flash 250 scanner (Perkin Elmer, Waltham MA). Scanned slides were viewed through the Pannormaic viewer software program (3D Histech, Waltham MA). An individual blinded to the experimental design captured JPEG images from 3 randomly chosen regions (each representing an area of 315 cm^2) from each slide at 20X magnification. Quantification of immunostaining on each JPEG was conducted using an automated analysis program with Matlab's image processing toolbox (Mathworks).

Supplementary figures

Figure S1

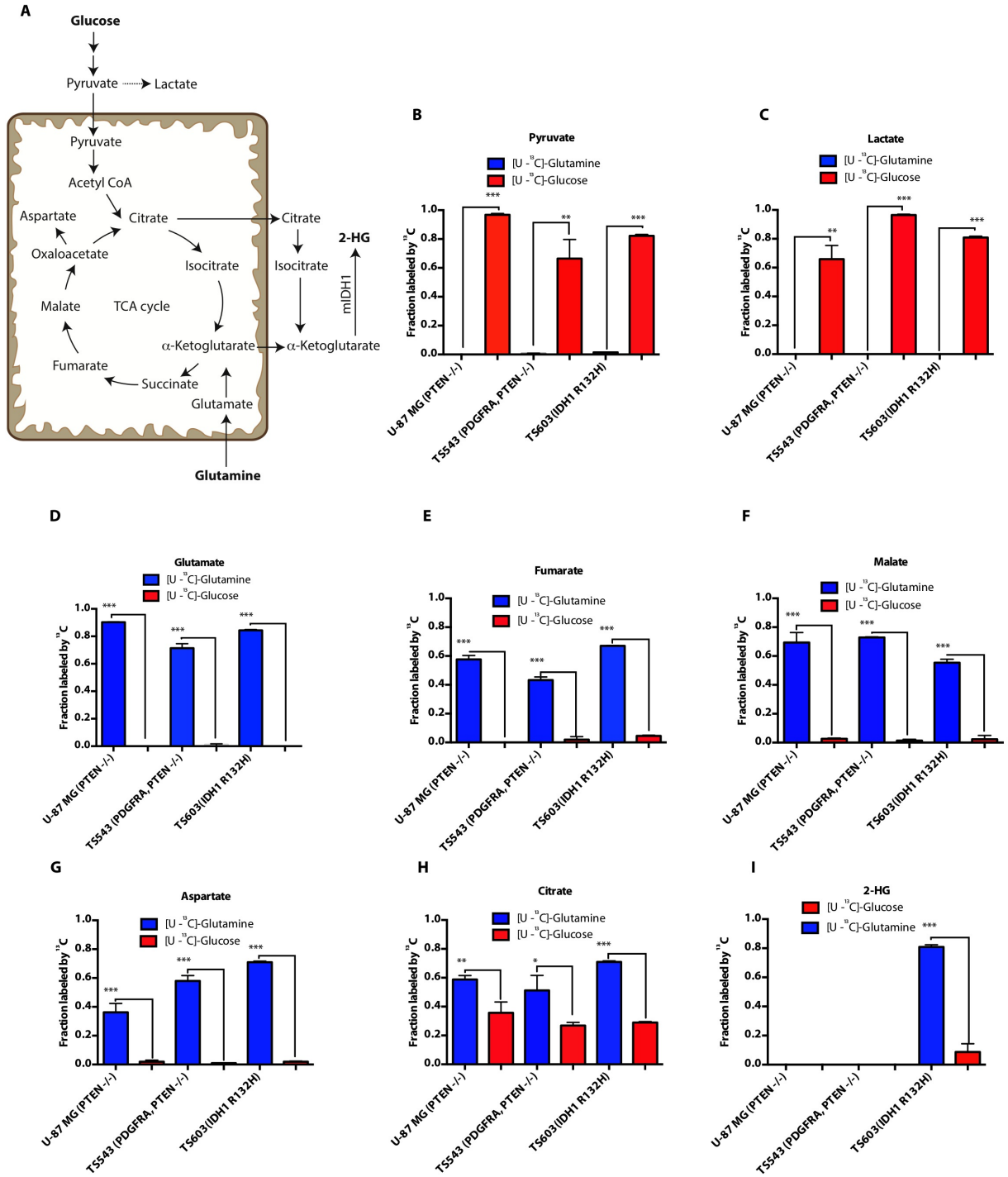

S1. Glutamine is a major TCA cycle substrate and generates 2-HG.

A. Model depicting glucose and glutamine metabolism in relationship to the TCA cycle and the generation of 2-HG from glutamine in IDH1 mutant glioma cell lines.

B-I. U-87 MG (PTEN -/-), TS543 (PDGFRA, PTEN -/-) or TS603 (IDH1 R132H) glioma cell lines were incubated with [U-^{13}C] – labeled glutamine or glucose. Pyruvate (B), lactate (C), glutamate (D), fumarate (E), malate (F), aspartate (G), citrate (H) and 2-HG (I) levels derived from either [U-^{13}C]-glutamine (blue bars) or [U-^{13}C]-glucose (red bars) were measured using GC-MS. Pyruvate and lactate were mainly derived from glucose consistent with the Warburg effect. Glutamate, fumarate, malate and aspartate were mainly derived from glutamine. Citrate was labeled with both [U-^{13}C]-glucose and [U-^{13}C]-glutamine with a significantly higher fraction from glutamine than that derived from glucose. 2-HG was detected only in TS603 (IDH1 R132H) mutant cells and was mainly labeled by [U-^{13}C]-glutamine. For all graphs, Data are represented as the mean ± standard deviation for n=3 independent experiments. Statistical significance was determined by two-sided, unpaired, Student's t-test. *p<0.05, **p<0.01, ***p<0.001.

Figure S2

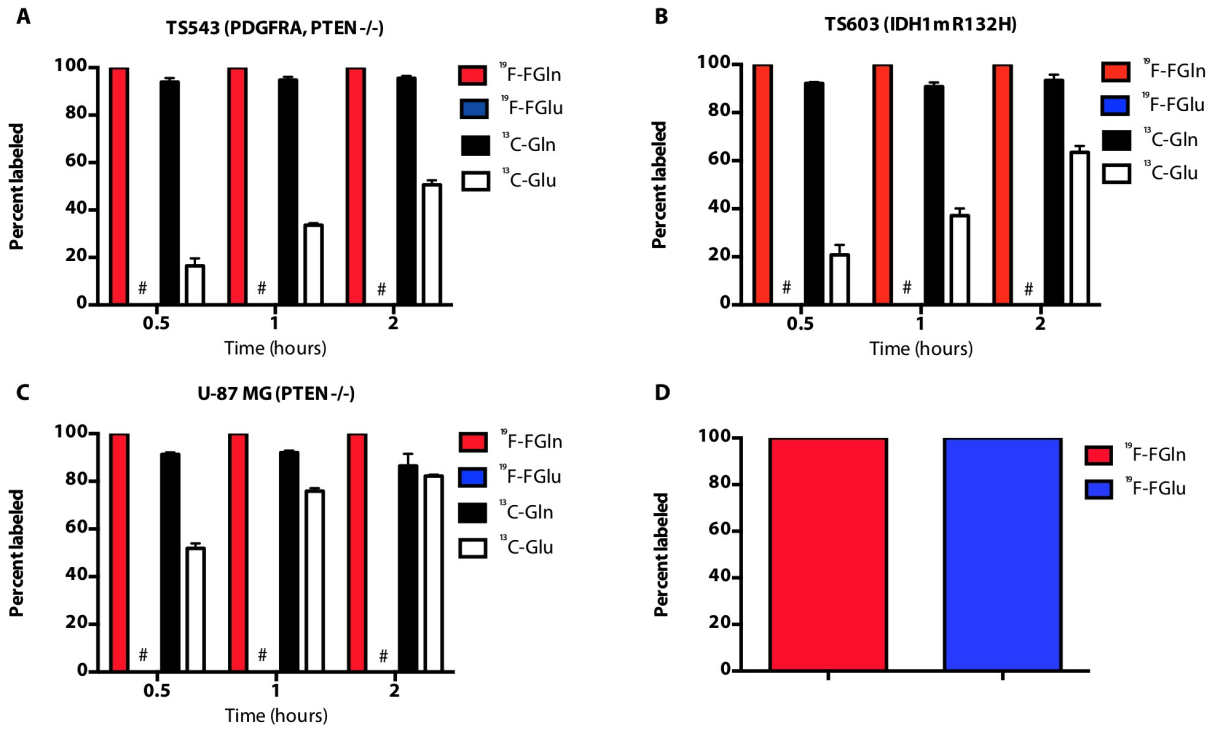

S2. ^{19}F-FGln is not metabolized in gliomas.

A-D. TS543 with PDGFRA amplification and PTEN deletion (A) and TS603 with IDH1 R132H mutation (B) and U-87 MG with PTEN deletion (C) glioma cell lines were incubated with 2 mM ^{19}F-glutamine (^{19}F-FGln) or 2 mM [U-^{13}C]-glutamine (^{13}C-Gln) for 0.5, 1 and 2 hours. ^{19}F-FGln (red bars), ^{19}F-glutamate (^{19}F-FGlu, blue bars), ^{13}C-Gln (black bars) and ^{13}C-glutamate (^{13}C-Glu, white bars) were measured using GC mass spectroscopy. # indicates that no ^{19}F-FGlu was detected in these conditions. For all graphs, Data are represented as the means ± s.e.m. for n=3 independent experiments. Pure ^{19}F-FGln (red bars) and ^{19}F-FGlu (blue bars) were run as standards for comparison (D).

Figure S3

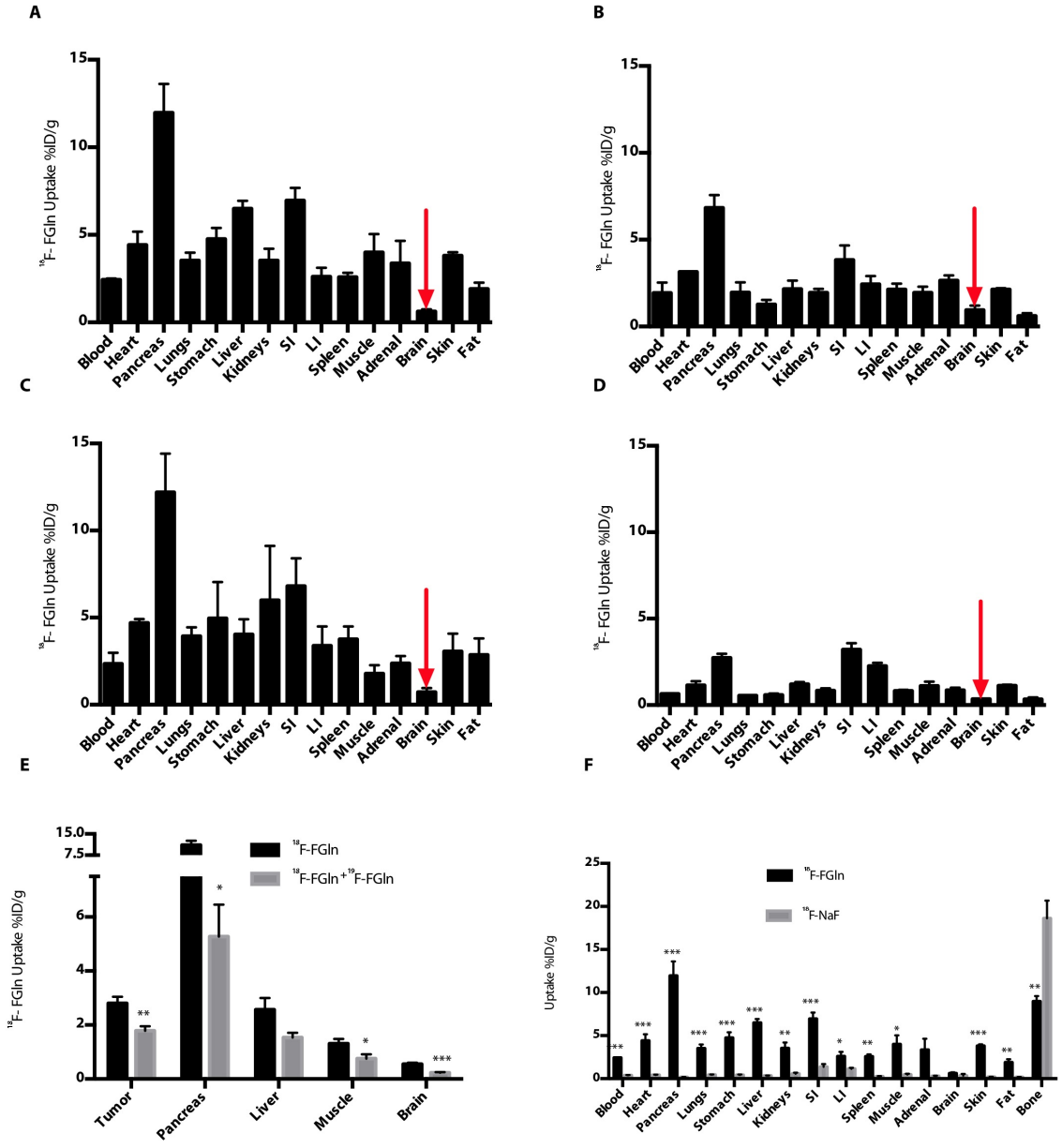

S3. ^{18}F-FGln shows minimal, but specific uptake in the normal brain.

A-D. ^{18}F-FGln was injected into the tail veins of normal mice. Various organs at 0.25 hr (A, n=4), 0.5 hr (B, n=4), 1 hr (C, n=4) and 2 hr (D, n=3) were harvested and weighed and their radioactive counts were measured on a gamma counter

and as percent of injected dose per gram of tissue (%ID/g). Red arrow indicates brain. SI = small intestine, LI = large intestine.

E. ^{18}F-FGln with or without excess ^{19}F-FGln was co-injected into the tail veins of mice bearing TS543 glioma xenografts. Glioma xenografts and other organs including the pancreas, liver, muscle and normal brain were harvested 1 hour later. ^{18}F-FGln uptake (%ID/g) was compared between the two conditions (for n=5 animals in each group).

F. ^{18}F-Sodium Fluoride (^{18}F-NaF) uptake in various organs was compared with ^{18}F-FGln at 0.5 hr post injection. SI = small intestine, LI = large intestine (for n=4 animals in each group).

For all graphs, Data are represented as the means ± s.e.m. Statistical significance was determined by two-sided, unpaired, Student's t-test; *p<0.05, **p<0.01, ***p<0.0001.

Figure S4

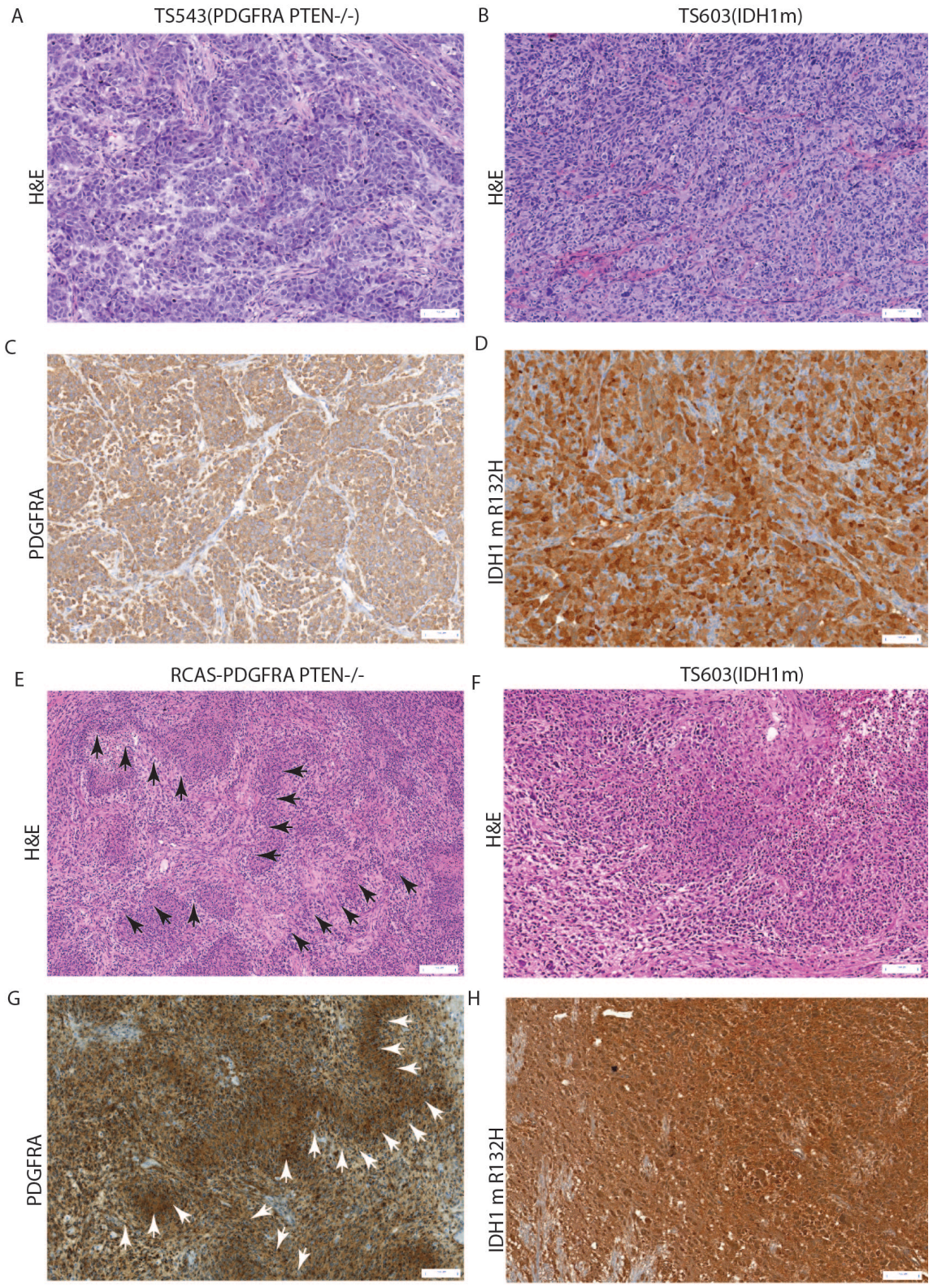
A
TS543(PDGFRA PTEN-/-)
B
TS603(IDH1m)
H&E
H&E
C
D
PDGFRA
IDH1 m R132H
E
RCAS-PDGFRA PTEN-/-
F
TS603(IDH1m)
H&E
H&E
G
H
PDGFRA
IDH1 m R132H

S4. Mouse glioma models mimic human gliomas.

A-B. Representative images from H&E sections (20X) from xenografts from animals subcutaneously implanted with TS543 (PDGFRA, PTEN -/-) (A) or TS603 (IDH1 R132H) (B) glioma cell lines.

C. Immunohistochemical stain (20X) for PDGFRA in TS543 (PDGFRA, PTEN -/-) subcutaneous xenograft tissues.

D. Immunohistochemical stain (20X) specific for mutant IDH1 R132H from TS603 (IDH1 R132H) subcutaneous xenograft tissues.

E-F. Representative images from H&E sections (20X) from RCAS-PDGF PTEN -/- (E) or animals implanted intracranially with TS603 (IDH1 R132H) glioma cell lines (F). Black arrows indicate areas with pseudopalisading necrosis.

G. Immunohistochemical stain (20X) for PDGFRA in RCAS-PDGF PTEN -/- animals. White arrows indicate areas with pseudopalisading necrosis.

H. Immunohistochemical stain (20X) specific for mutant IDH1 R132H from TS603 (IDH1 R132H) orthotopic implanted mice.

Figure S5

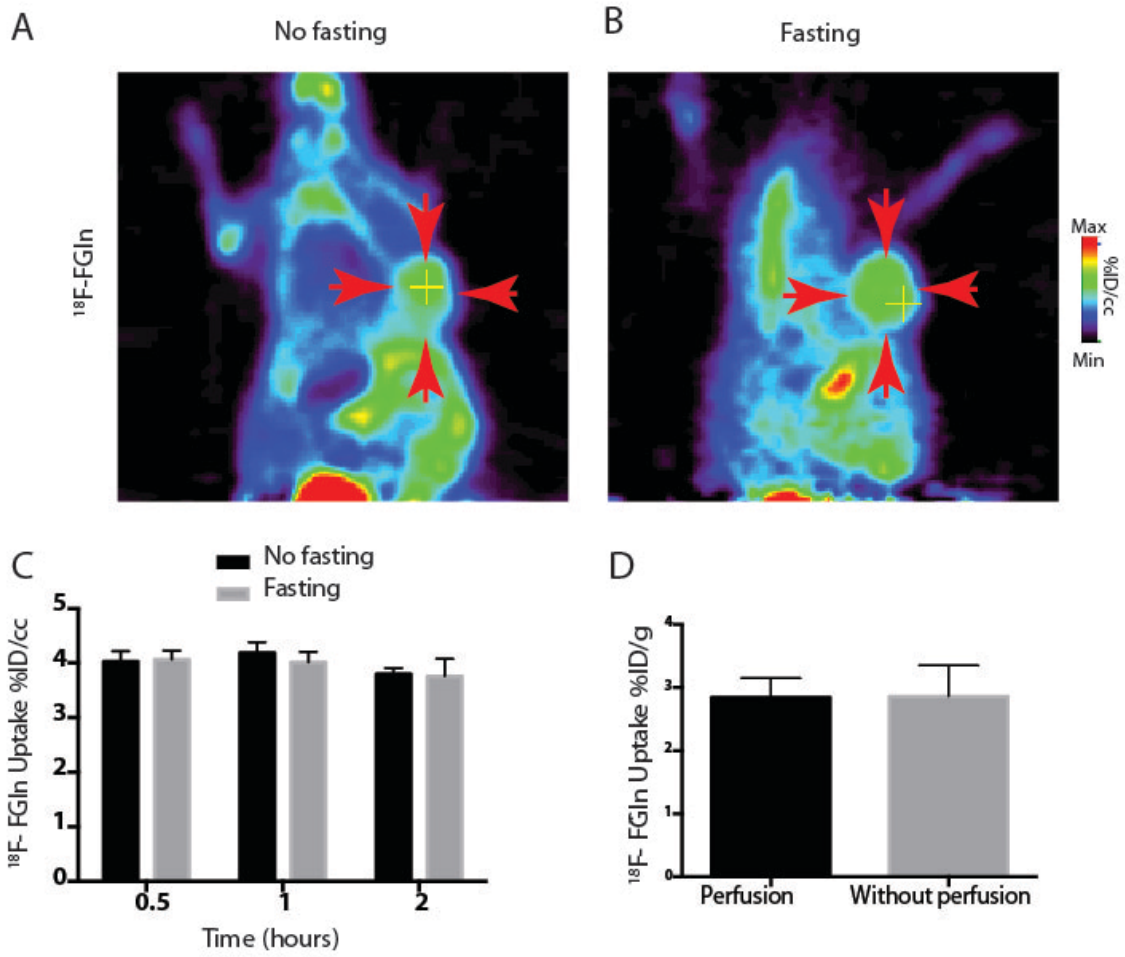

S5. Fasting and perfusion do not affect ^{18}F-FGln uptake.

A-B. Representative coronal ^{18}F-FGln PET images from mice bearing U-87 MG xenografts after fasting for 12 hours (A) or without fasting (B).

C. Comparison of ^{18}F-FGln uptake in animals fasted for 12 hours (gray bars, n=5) with animals not fasted (black bars; n=4). Statistical significance was determined by Wilcoxon matched-pairs signed rank *t* test. %ID/cc: percent-injected dose/ cubic centimeter.

D. Comparison of ^{18}F-FGln uptake 30 mins post injection in mice bearing U-87 MG xenografts with (gray bars) or without perfusion (black bars; n=3, each

group). Statistical significance was determined by two-tailed, Student's t-test.

%ID/cc: percent-injected dose/ cubic centimeter.

For all graphs, Data are represented as the means ± s.e.m,

Figure S6

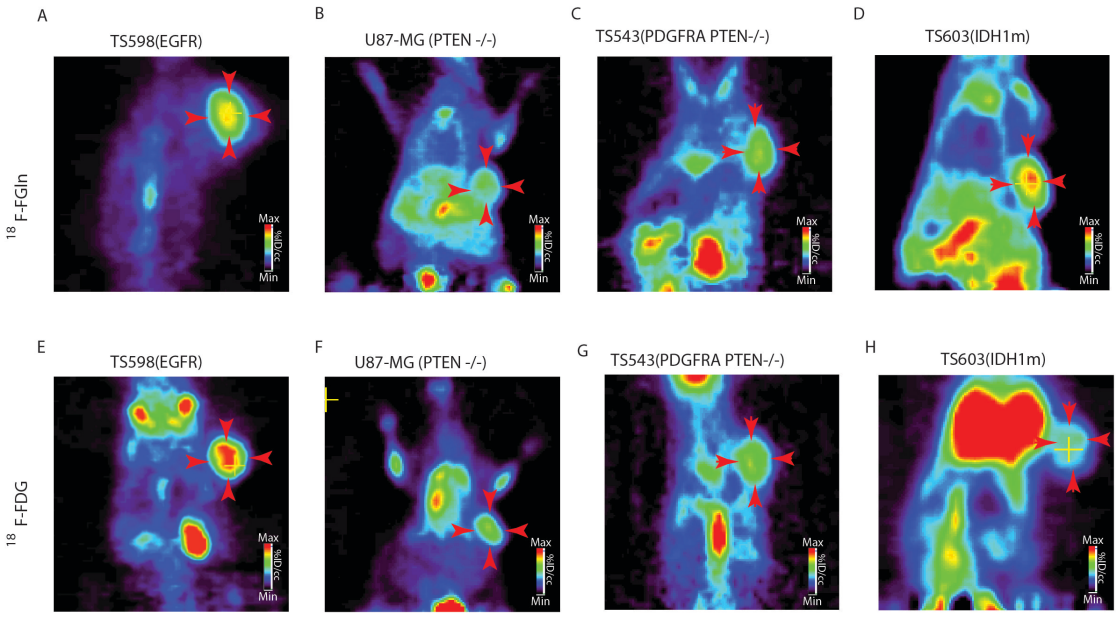

S6. ^{18}F-FGln shows uptake in mouse glioma xenografts.

A-D. Representative full body coronal PET images showing ^{18}F-FGln uptake in TS598 (EGFR) (A), U-87 MG (PTEN -/-) (B), TS543 (PDGFRA, PTEN -/-) (C) or TS603 (IDH1 R132H) (D) glioma xenografts (indicated by red arrows).

E-H. Representative full body coronal PET images showing ^{18}F-FDG uptake in TS598 (EGFR) (E), U-87 MG (PTEN -/-) (F), TS543 (PDGFRA, PTEN -/-) (G) or TS603 (IDH1 R132H) (H) glioma xenografts (indicated by red arrows).

Figure S7

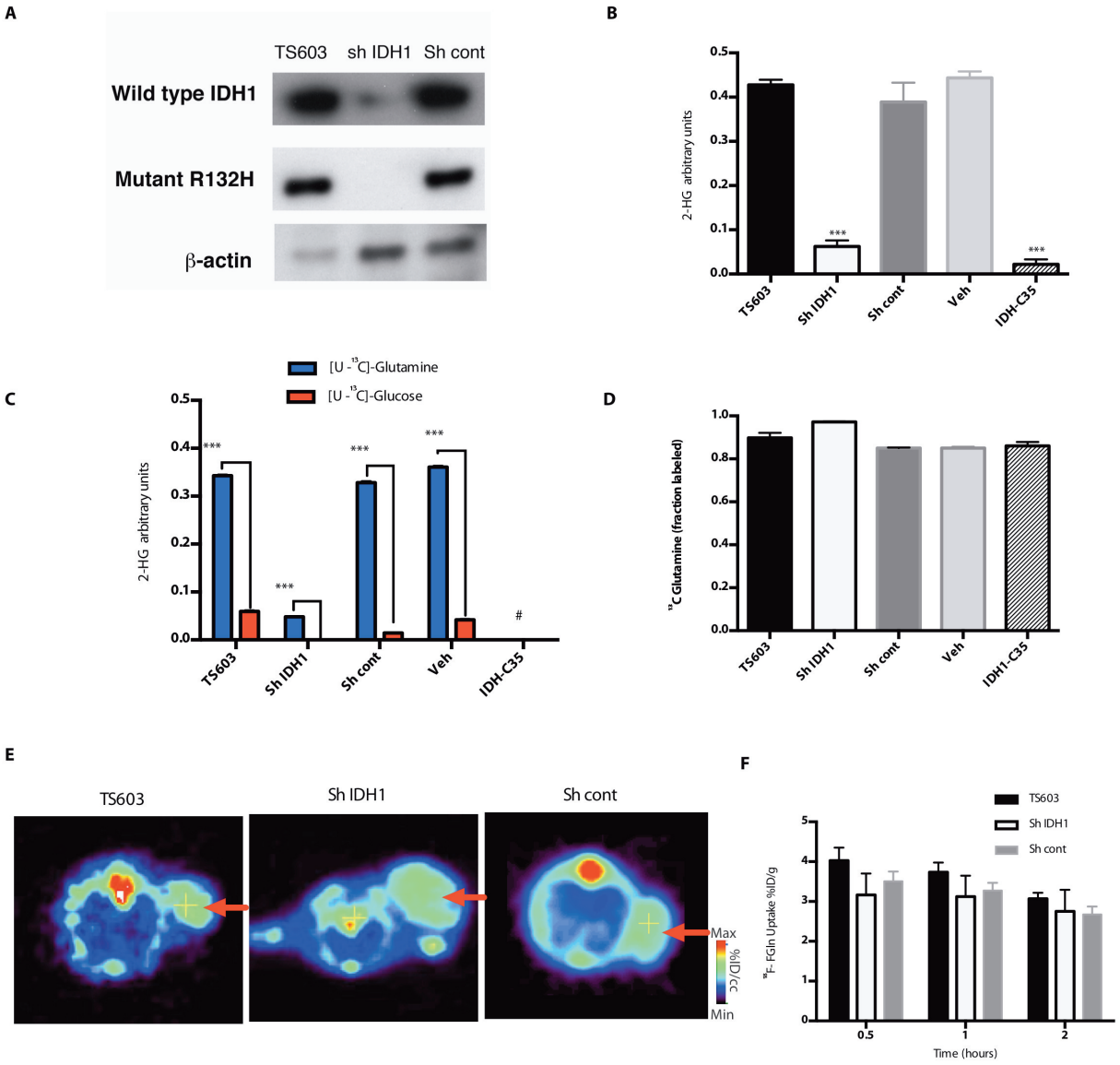

S7. Gln is metabolized to 2-HG without altering ^{18}F-FGln uptake.

A. Western blots in TS603 (IDH1 R132H) glioma cell lines with (sh IDH1) or without (empty vector control = Sh control) shRNA targeted against total IDH1, probed with antibodies against wild type IDH1 (top panel), or mutant IDH1 R132H (middle panel), or β-actin as loading control (bottom panel).

B. 2-HG levels were measured using GC-MS in TS603 (IDH1 R132H) cells with (white bars - Sh IDH1) or without (gray bars - Sh control, black bars - control untreated) shRNA against total IDH1. Cells were also treated with vehicle (Veh- light gray bars) or an IDH1 mutant specific inhibitor (IDH1-C35, 1500 nM for 48 hr, dotted bars).

C. 2-HG derived from either [U-^{13}C]-glutamine (blue bars) or [U-^{13}C]-glucose (red bars) were measured using GC-MS in similar experimental conditions described in B. # indicates that no ^{13}C-labeled 2-HG was detected in this condition.

D. Fraction of [U-^{13}C]-glutamine labeled in similar experimental conditions as in B.

E. Representative transverse ^{18}F-FGln PET images (1 hour post injection) from TS603 (IDH1 R132H) xenografts (red arrows) with (Sh IDH1) or without (Sh cont, control) shRNA against total IDH1.

F. ^{18}F-FGln uptake in TS603 (IDH1 R132H) xenografts (black bars, n=5) with (Sh IDH1, clear bars; n=3) or without (gray bars; Sh cont, n=5) shRNA against total IDH1. %ID/cc: percent-injected dose/ cubic centimeter.

For all graphs, data are represented as mean ± s.e.m. for at least n=3 independent experiments. Statistical significance was determined by two-sided, unpaired Student's t-test or ANOVA; *p<0.05, **p<0.01, ***p<0.0001.

Figure S8.

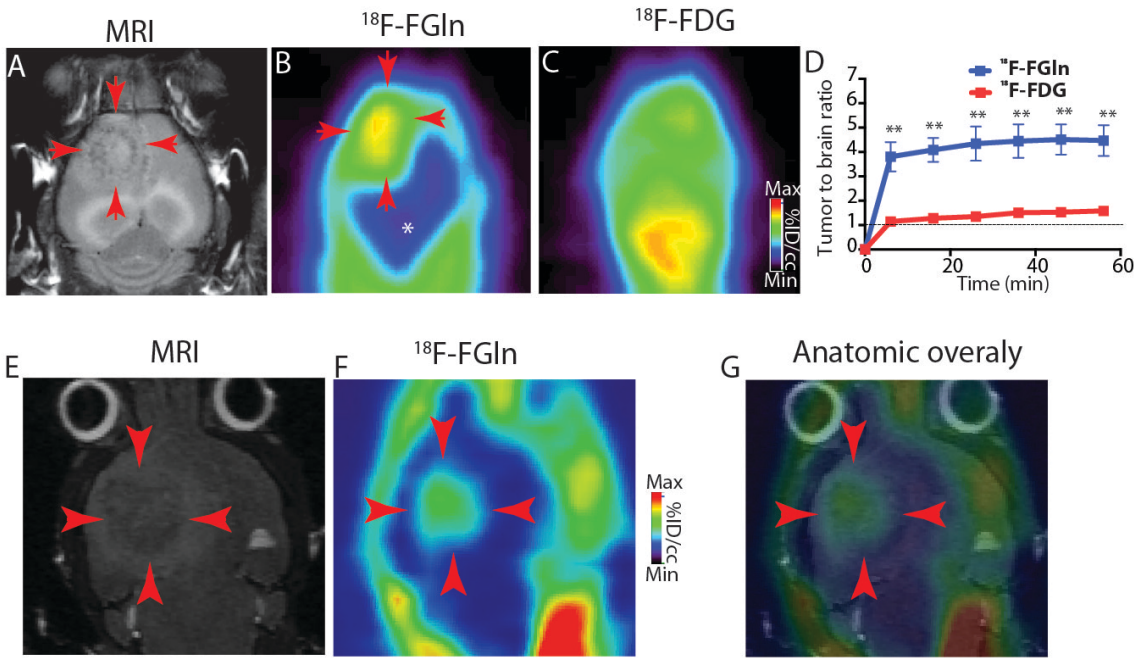

S8. Glioma animal models show ^{18}F-FGln tumor uptake.

A. Representative coronal MRI from RCAS-PDGF, PTEN wild type mouse depicting tumor (red arrows).

B. Coronal ^{18}F-FGln PET image from the same mouse illustrating high tumor (red arrows) uptake compared to surrounding non-neoplastic brain (white asterisk).

C. Coronal ^{18}F-FDG PET image from the same animal depicting poor tumor delineation.

D. Time activity curve illustrating tumor to background ratio with ^{18}F-FGln (blue line, n=5) compared to ^{18}F-FDG (red line, n=5) in RCAS-PDGF PTEN wild type animals. Dotted black line indicates an equal tumor to brain ratio of 1:1. For all

graphs, Data are represented as the means ± s.e.m. , statistical significance was determined by two-sided, unpaired, two-tailed, Student's t-test; ** $p<0.01$. **E-G.** Anatomic overlay (G) of MRI (E) and ^{18}F-FGln PET (F) from a TS603 IDH1m mouse indicating ^{18}F-FGln uptake in the tumor (red arrows) distinct from the surrounding brain and skull.

Figure S9

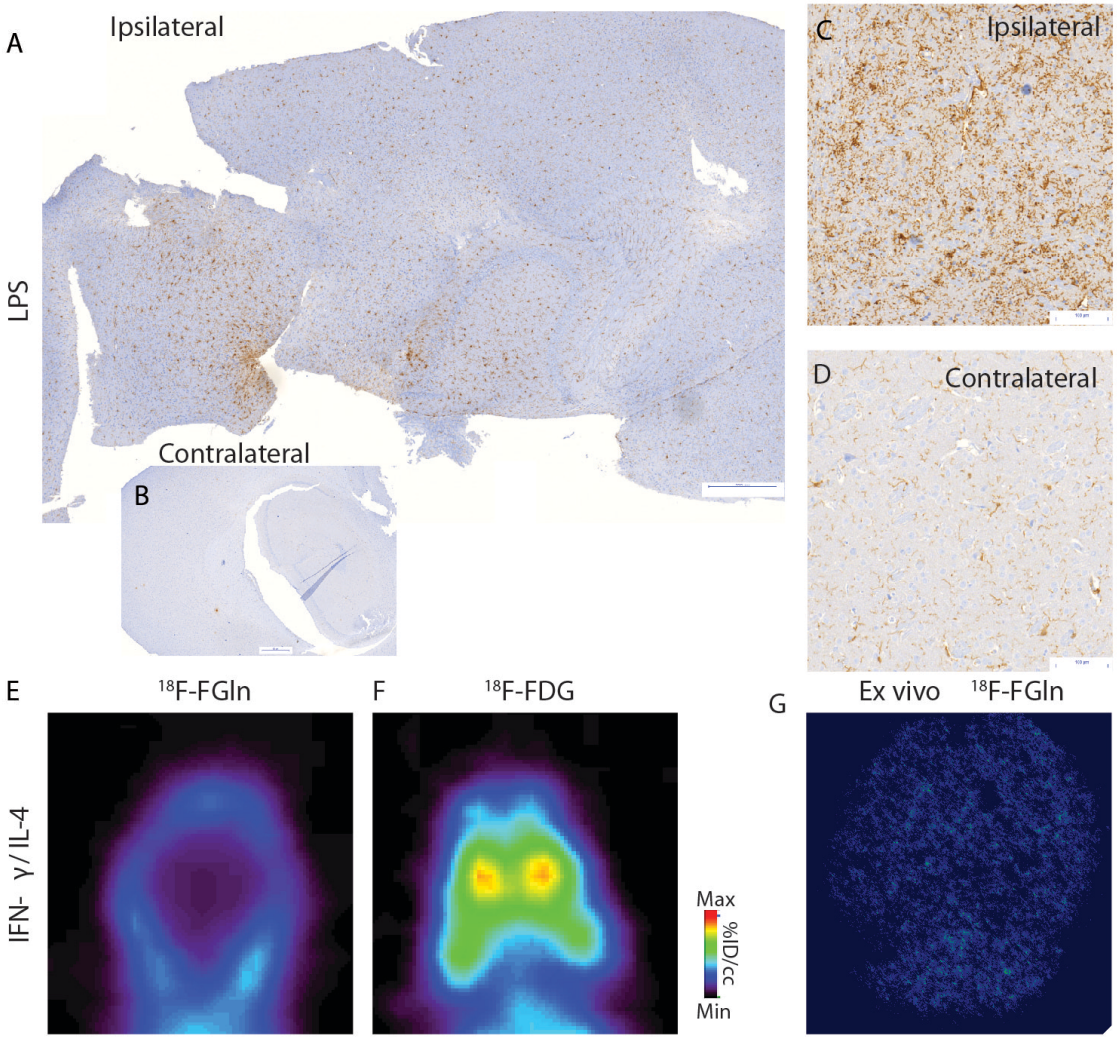

S9. Neuroinflammatory mouse models do not show ^{18}F-FGln uptake.

A-B. Representative image of IBA1 (labeling activated microglia and macrophages) immunostaining (5X) from an animal injected with LPS (ipsilateral side (A) depicting IBA1 positive cells throughout the hemisphere; contralateral side (B) showing minimal immunoreactivity).

C-D. Representative high power (40x) images of IBA1 from an animal injected with LPS on the ipsilateral (C) and contralateral (D) sides of injection.

E. Representative coronal ^{18}F-FGln PET image from an animal injected with IFN-γ/ IL-4.

F. Coronal ^{18}F-FDG PET image from the same animal.

G. Representative ex-vivo ^{18}F-FGln autoradiogram from the same animal.

Figure S10

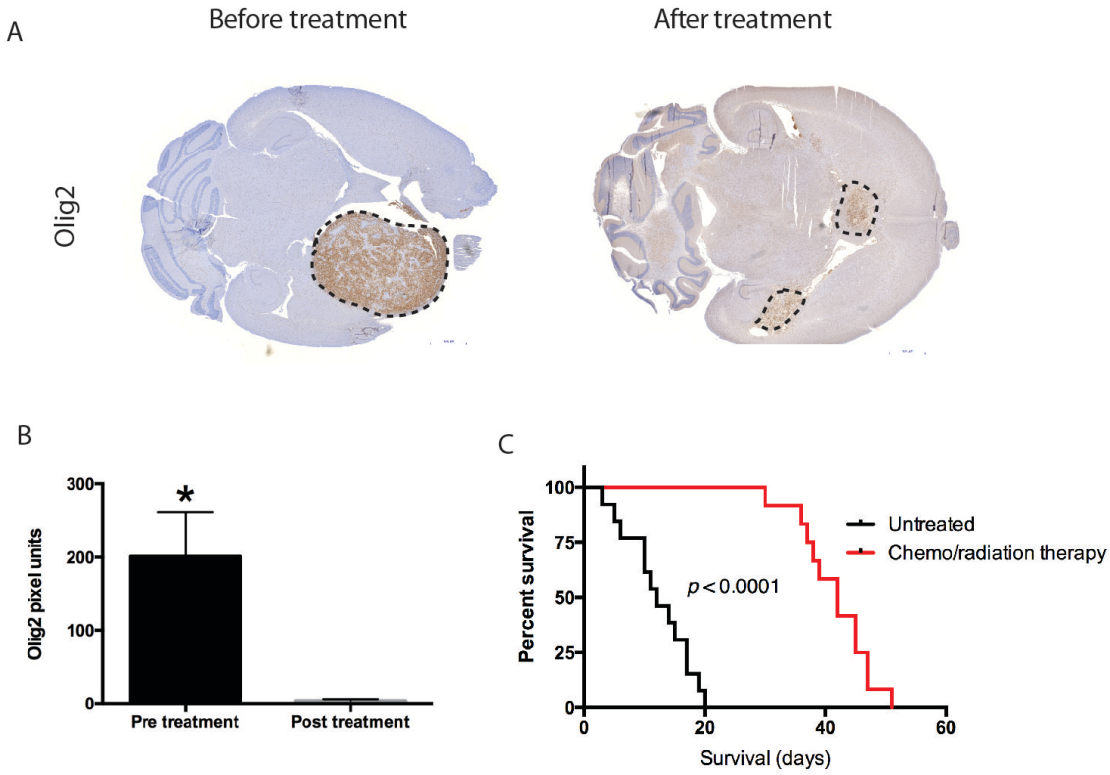

S10. Chemoradiation decreases tumor burden and improves survival.

A-B. Representative images (A) and corresponding quantification (B) of Olig2 (labeling tumor cells, 2X, A). For all graphs, Data are represented as the means ± s.e.m., statistical significance was determined by two-sided, unpaired, two-tailed, Student's t-test; *p<0.05.

C. Kaplan-Meier curve in chemo/radiation therapy treated mice (n=12, red) showing improved survival compared to untreated mice (n=14, black). Differences in survival were determined using the Log-Rank test (p<0.0001).

Figure S11

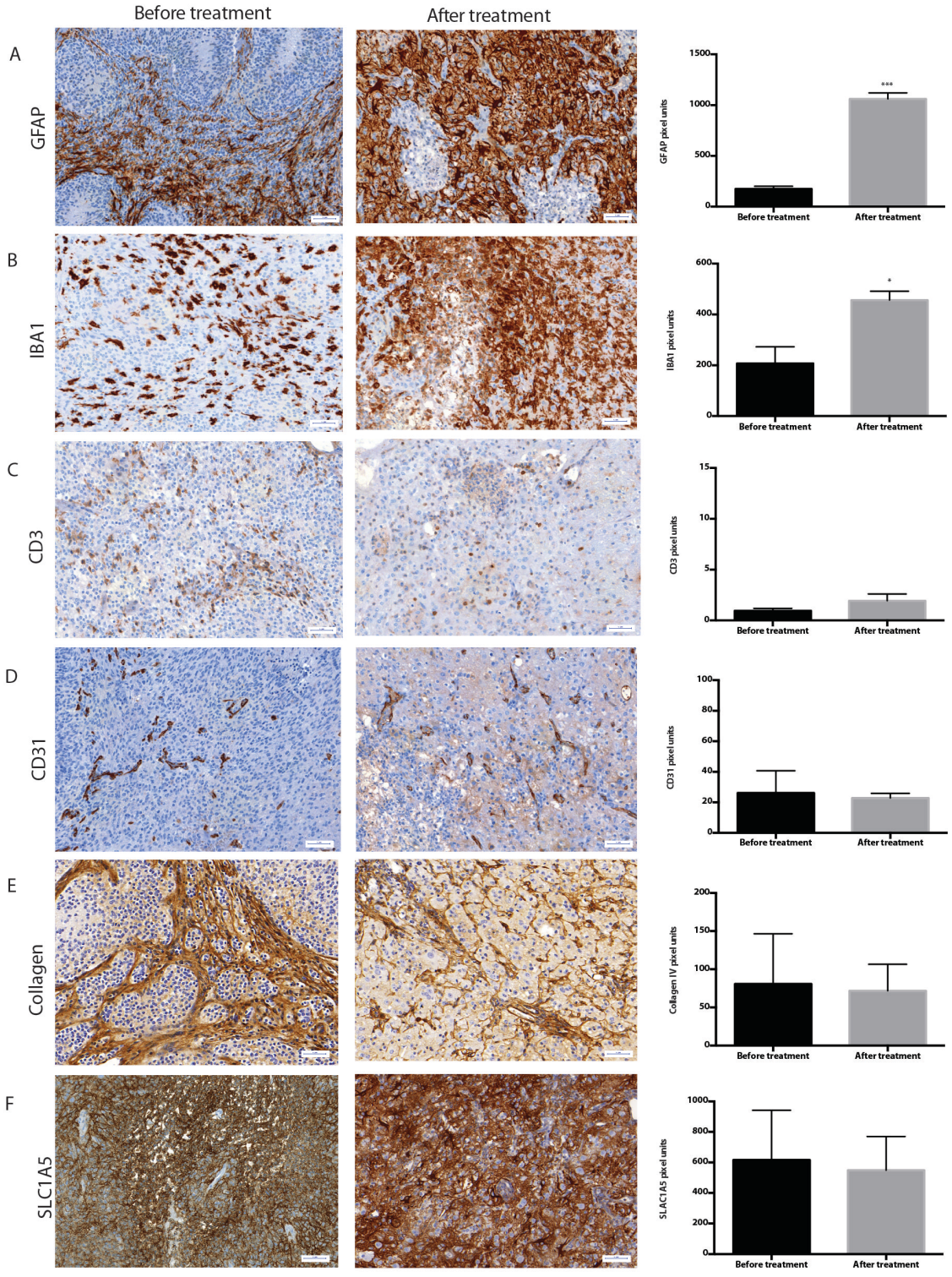

S11. Chemoradiation therapy results in increased gliosis.

A-F. Representative images and corresponding quantification of GFAP (reactive astrocytosis, 40X, A), IBA1 (activated macrophages and microglia, 40X, B), CD3 (labeling lymphocytes, 40X, C), CD31 (endothelial cells, 40X, D), collagen (vessel walls, 40X, E) and SLC1A5 (glutamine transporter, 40X, F) in animals pre treatment (n=3) and animals post treatment (n=4). Scale bars represent 100 μM. For all graphs, Data are represented as the means ± s.e.m., statistical significance was determined by two-sided, unpaired, two-tailed, Student's t-test; **p*<0.05, ****p*<0.001.

Figure S12

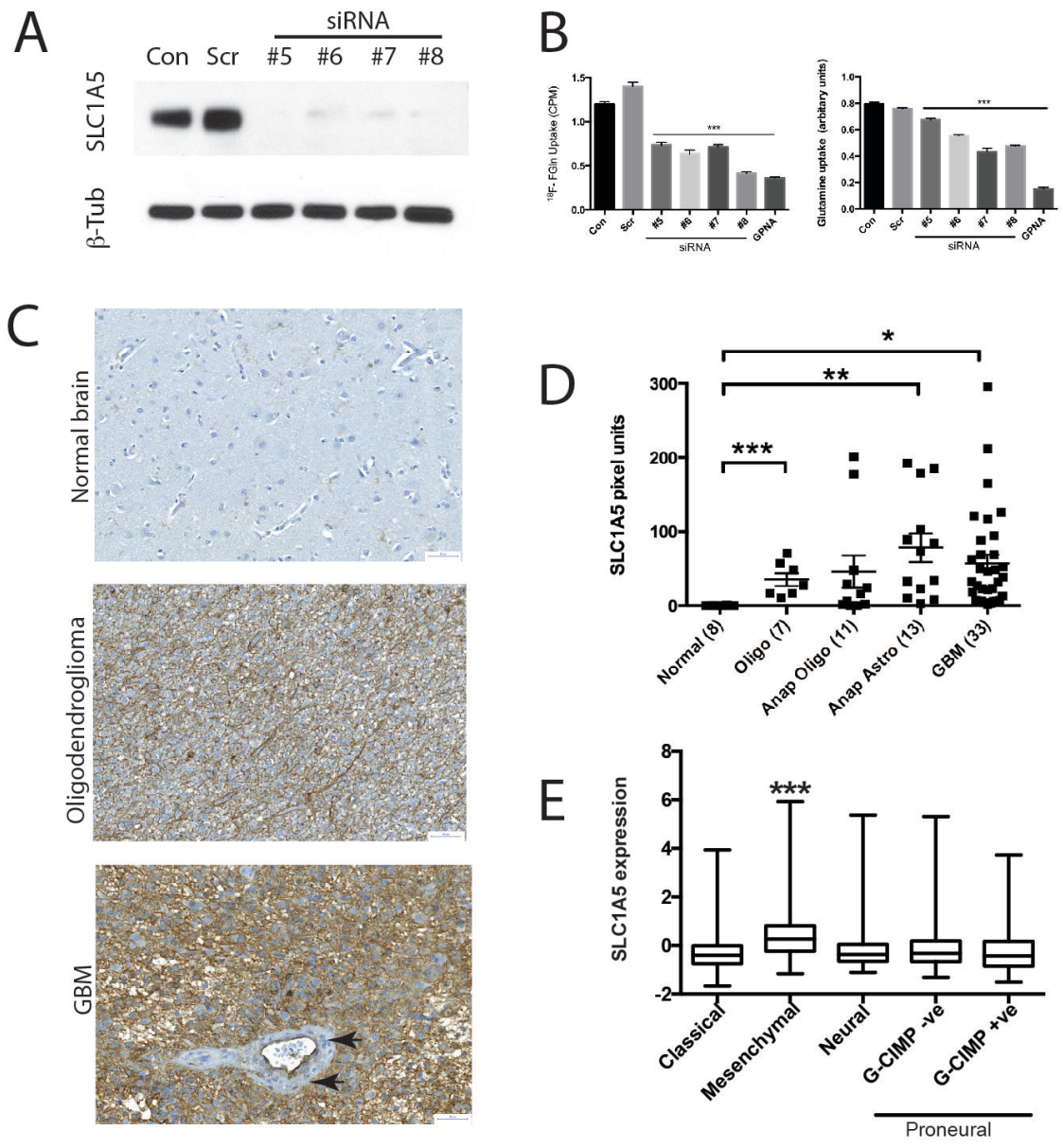

S12. SLC1A5 partly mediates ^{18}F-FGln uptake and is expressed in human gliomas.

A. Knockdown of SLC1A5 after transfection of siRNAs (4 different siRNAs #5, #6, #7 and #8) targeted against SLAC1A5 in SF188 glioma cell lines. Scrambled (Scr) siRNA was used as control. β-Tub (β-tubulin as loading control).

B. Both ^{18}F-FGln and glutamine show decreased uptake upon siRNA knockdown of SLC1A5 or treatment with the SLC1A5 inhibitor GPNA.

C. Representative images (40X) from normal brain, oligodendroglioma and GBM immunostained for SLC1A5. Arrows point to negative staining in blood vessels used as internal negative control.

D. Quantification of SLC1A5 expression in normal brain (n=8) compared to glioma patient samples with WHO grade II oligodendrogliomas (Oligo, n=7), grade III anaplastic oligodendrogliomas (Anap Oligo, n=11), grade III anaplastic astrocytomas (Anap Astro, n=13) and grade IV GBMs (n=33).

E. SLC1A5 mRNA expression from the cancer genome atlas (TCGA) in different subgroups of GBM.

Data are represented as mean ± s.e.m, statistical significance was determined using ANOVA; *p<0.05, **p<0.01, ***p<0.0001.

Figure S13

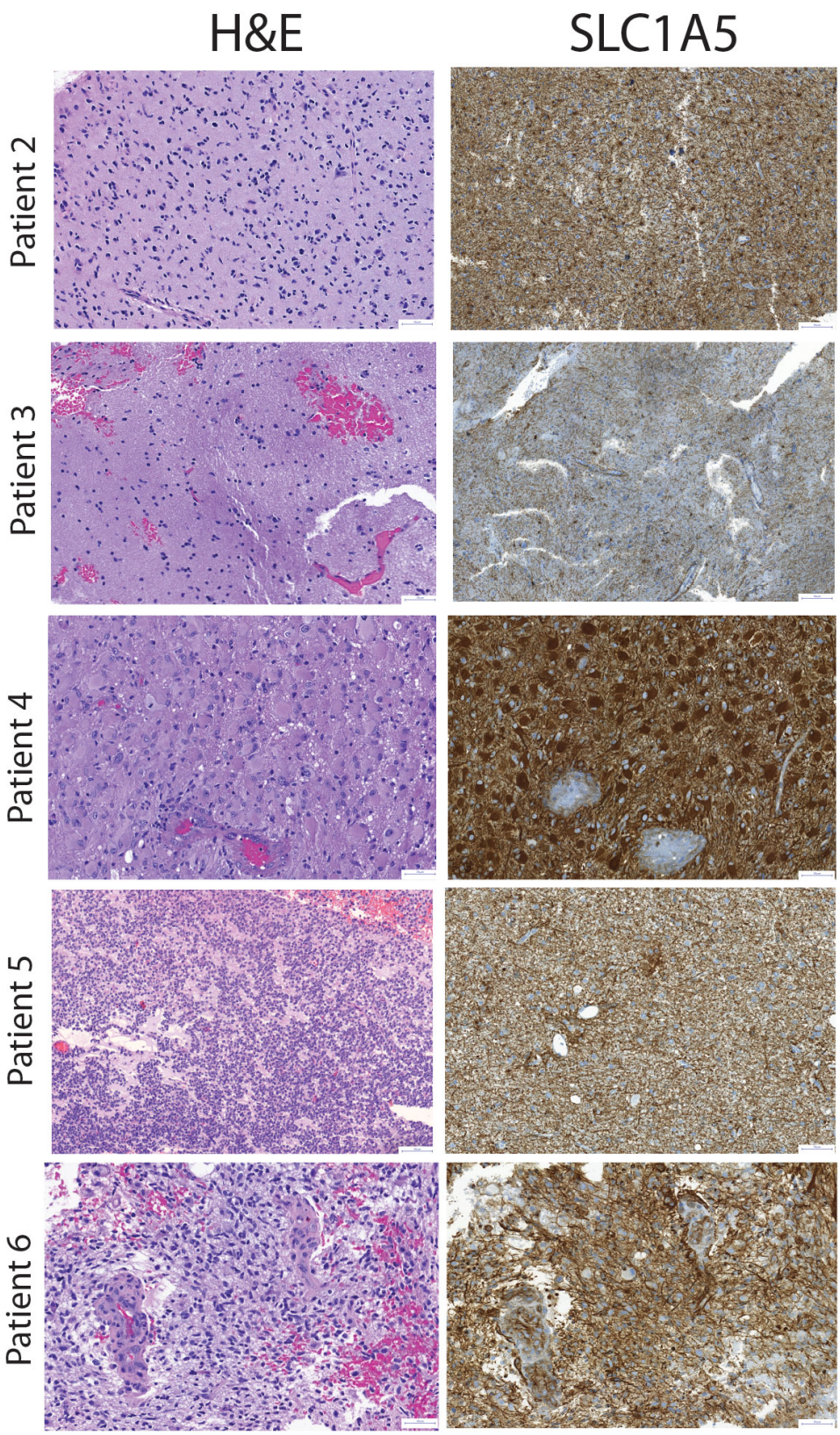

S13. Patients imaged with ^{18}F-FGln show glioma SLC1A5 expression.

Representative H&E and SLC1A5 immunostained images (40X) from patients 2-6 (tissue from patient #1 was not available). Histopathology, including SLC1A5 expression, was assessed in tissue samples available. In patient #2, this was on the grade II oligoastrocytoma biopsied 3.8 years ago; patient #3, grade II oligoastrocytoma biopsied 5.6 years back; patient #4, grade III recurrent/residual high-grade astrocytoma biopsied immediately after PET imaging; patient #5, grade II oligodendroglioma (which showed hypercellularity as illustrated, without necrosis or microvascular proliferation, suggestive of higher biologic potential than that associated with a WHO grade II lesion) biopsied 4.5 years back and patient #6, grade IV GBM biopsied 0.8 years back. Due to time differences between biopsy and imaging, no direct conclusions can be drawn between histopathology, SLC1A5 expression and imaging studies except in patient #4 where biopsy was obtained immediately after imaging.

Figure S14.

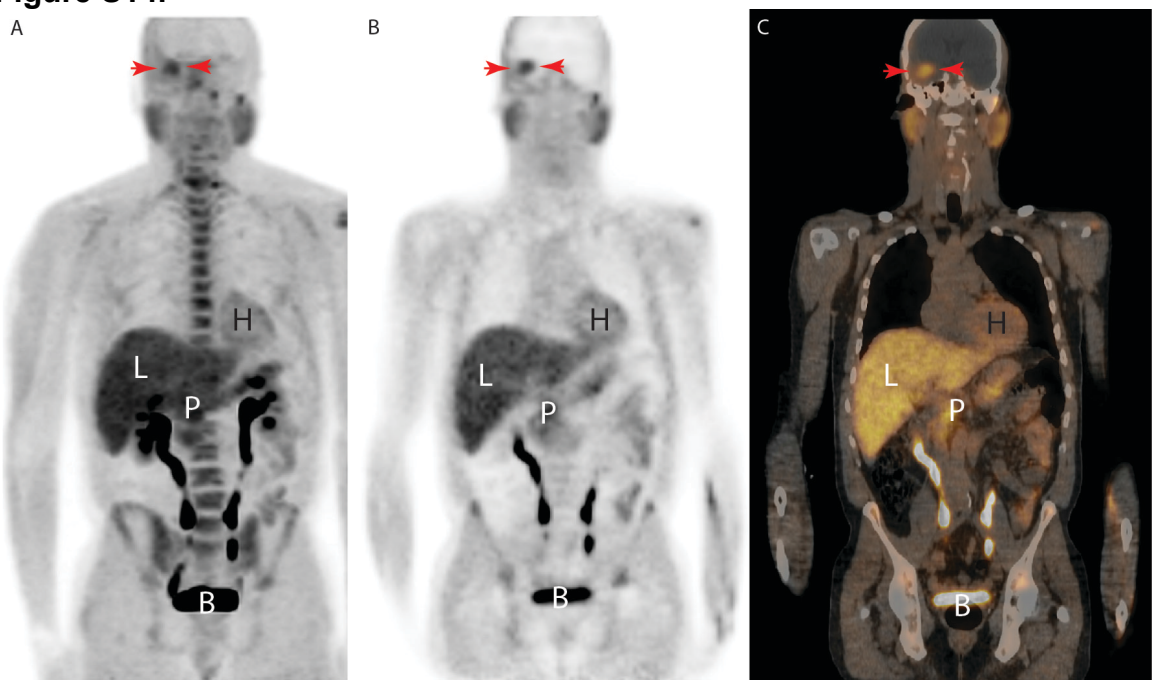

S14. ^{18}F-FGln shows uptake in a clinically progressive glioma.

A-C. 3-D maximum intensity projection (MIP) PET (A), coronal PET (B), and coronal fusion PET-CT images (C) from patient #6 with GBM (red arrows); H = heart, L = liver, P = pancreas, B = bladder. Images obtained 60 minutes post-injection of 468 MBq ^{18}F-FGln. Urinary excretion of tracer was evident but not hepatobiliary excretion . 75.6 +/- 8% of injected dose was excreted via urinary tract by the last PET time-point (range: 60.6% - 83.2%) tracer was present in the urinary tract or absent from the PET field of view (and assumed excreted via urinary tract) by 2-3 hours after tracer-injection.

Figure S15

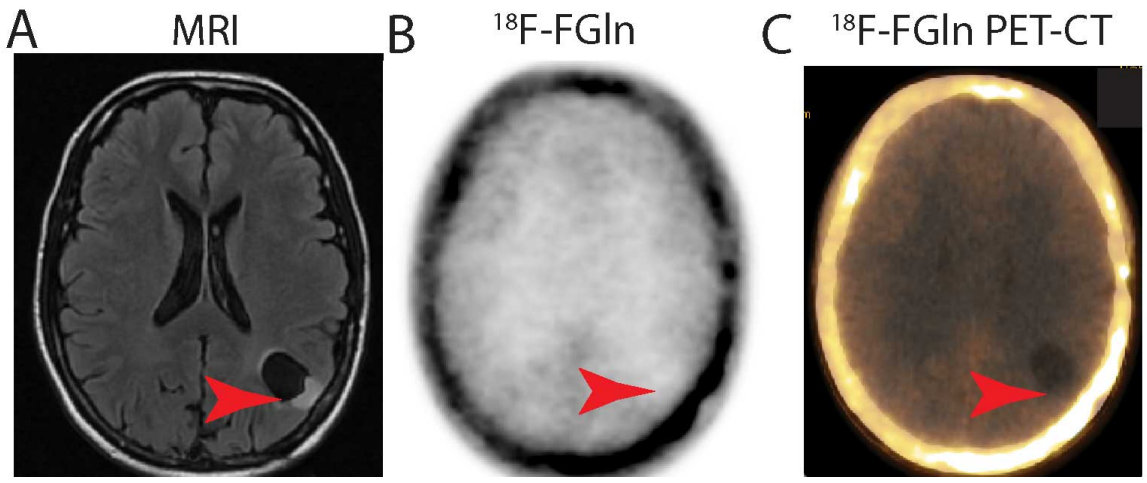

S15. ^{18}F-FGln does not show uptake a clinically stable glioma.

A. T1-weighted fluid attenuation inversion recovery (FLAIR) MRI from patient #2: a 37-year-old female with IDH1 mutant oligoastrocytoma, grade II (red arrow).

B. ^{18}F-FGln PET showing no uptake in tumor.

C. Fusion ^{18}F-FGln PET-CT showing no ^{18}F-FGln uptake in area corresponding to tumor (red arrow).

Figure S16

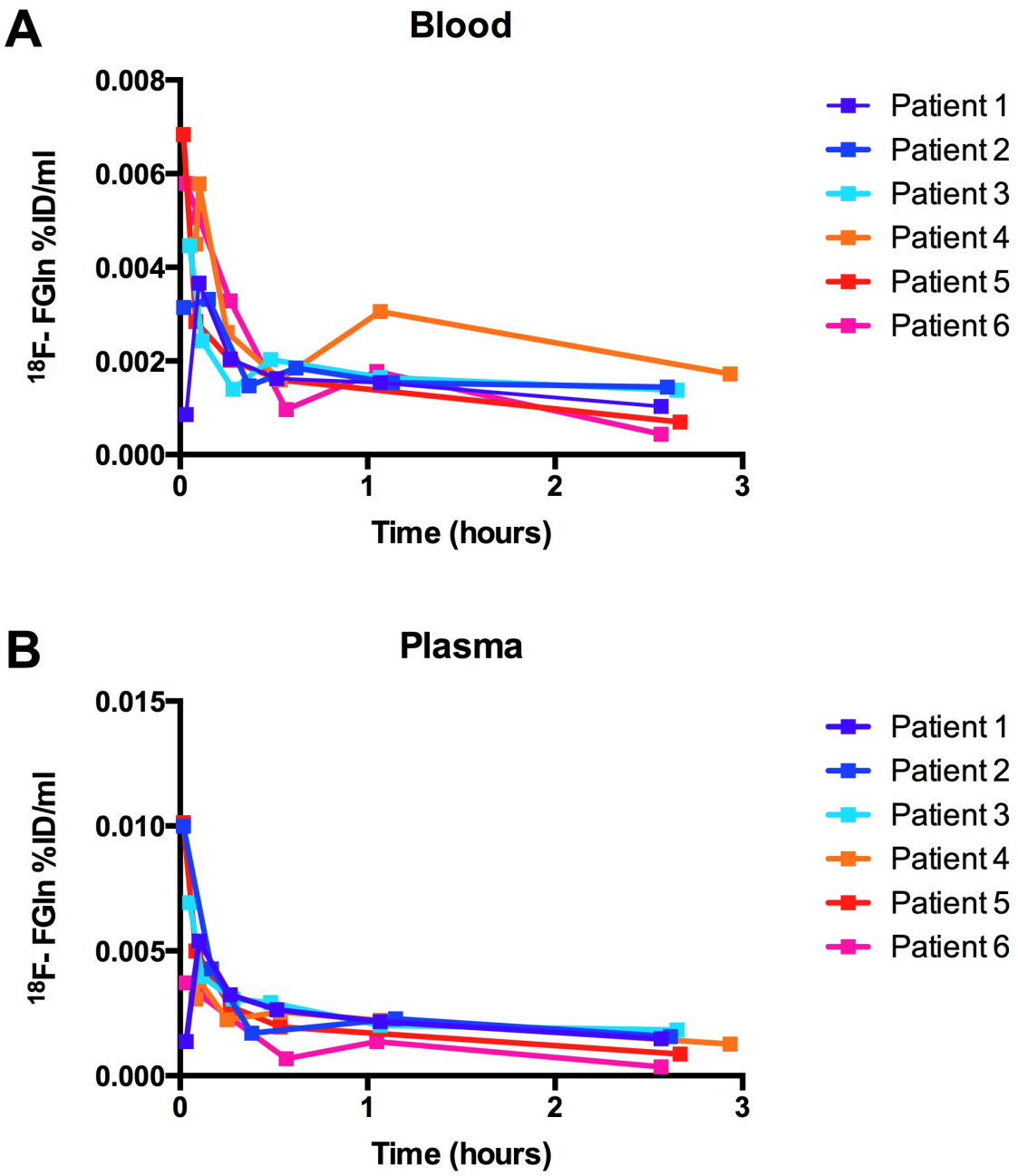

S16. ^{18}F-FGln shows clearance from blood and plasma.

Shown are blood (A) and plasma (B) activity concentrations at multiple time-points up to 3 hours after bolus intravenous injection of ^{18}F-FGln. Y-axis

represents activity concentration as a percentage of the injected dose per mL of blood or plasma (%ID/mL). X-axis represents hours after tracer-injection. Each data point represents total sample activity, including parent compound and radio-metabolites. ^{18}F-FGln cleared from the blood and plasma in a biexponential pattern, with initial phase clearance half-times of 0.04 ±0.02 h and 0.03 ±0.02 h and terminal clearance half-times of 2.6 ±1.2 h and 3.0 ±1.2 h, respectively.

Supplementary Tables

CLINICALLY STABLE PATIENTS

#	Age	Sex	Histology	Molecular characteristics	Prior Treatment type & last dose (mos.)	Follow up period since diagnosis
1	54	M	Oligo-astrocytoma	IDH WT, MGMT methylated, 1p/1q intact	Poly-ICLC . stopped 2 mos prior	3.8 yrs
2	37	F	Oligo-astrocytoma	IDH1 R132H mutant, 1p/1q intact	Temozolomide. stopped 11 mos prior	5.6 yrs
3	71	F	Astrocytoma	IDH1 R132H mutant, MGMT methylated	No treatment	1.5 yrs

PATIENTS WITH DISEASE PROGRESSION

#	Age	Sex	Histology	Molecular characteristics	Prior Treatment type & last dose (mos.)	Follow up period since diagnosis
4	53	F	Astrocytoma	IDH WT, EGFRvIII mutation, EGFR amplified	chemoradiation. stopped 14 mos prior.	2.4 yrs
5	42	M	Oligodendroglioma	IDH1 R132H mutant, 1p/19q deleted	No treatment	4.5 yrs
6	57	M	Glioblastoma	IDH WT, MGMT not methylated	Temozolomide (started after PET scan). Chemoradiation stopped 3 mos prior.	0.8 yrs

Table S1. Patient characteristics

Three clinically stable and three patients with clinically progressive disease were part of this study. MGMT (O-6-methylguanine DNA methyltransferase), Poly-ICLC (immunostimulant, consisting of carboxymethylcellulose, polyinosinic-polycytidylic acid and poly-L-lysine double stranded RNA), IDH1 (Isocitrate dehydrogenase 1), WT (wild type), EGFR (Epidermal growth factor receptor).

Table S2

CLINICALLY STABLE PATIENTS				^{18}F-FGln SUV max			^{18}F-FDG SUV max		
#	Histology	Grade	Size Prior to PET	Tum: Brain	Tum	Brain	Tum: Brain	Tum	Brain
1	Oligoastrocytoma	II	Slight Increase (yrs)	**1**	0.5	0.5	**0.9**	13.4	14.8
2	Oligoastrocytoma	II	Stable (yrs)	**1**	0.4	0.4	**0.3**	3	8.6
3	Astrocytoma	II	Stable (yrs)	**1.3**	0.8	0.6	**NA**	NA	NA

PATIENTS WITH DISEASE PROGRESSION				^{18}F-FGln SUV max			^{18}F-FDG SUV max		
#	Histology	Grade	Size Prior to PET	Tum: Brain	Tum	Brain	Tum: Brain	Tum	Brain
4	Astrocytoma	Lesion #1: transformed high-grade III (biopsy confirmed after imaging)	Increased	**4.2**	2.5	0.6	**NA**	NA	NA
	Astrocytoma	Lesion #2: transformed high-grade (clinical*)	Increased	**3.7**	2.2	0.6	**NA**	NA	NA
	Astrocytoma	Lesion #3: Background infiltrative (presumed still low-grade)	Stable (yrs)	**1**	0.7	0.7	**0.6**	6	10.5
5	Oligodendroglioma	Lesion #1: II/transformed (clinical**)	Increased	**4.6**	2.3	0.5	**0.9**	15.5	15.9
		Lesion #2: Presumed low-grade glioma (no biopsy)	Stable (yrs)	**1**	0.5	0.5	**0.2**	3.2	15.9
6	Glioblastoma	IV (on initial biopsy)	Increased	**4.8**	1.9	0.4	**0.9**	12	13.8

Table S2. Comparison of ^{18}F-FGln and ^{18}F-FDG imaging in human subjects.

Tum (Tumor, defined by correlation with brain MRI), SUV (standardized uptake value), *clinical diagnosis of transformed disease based upon tumor growth/enhancement on MRI (developed anew within 4 month period; within extensive infiltrative mass in left hemisphere), **clinical diagnosis of transformed disease based upon tumor growth on MRI**.** SUV values with ^{18}F-FGln were lower than those observed with ^{18}F-FDG in high-grade lesions. However, ^{18}F-FDG showed higher or similar values in the surrounding brain compared to tumors. Since gliomas lack margins and infiltrate into the surrounding brain, contributions to ^{18}F-FDG SUV values from tumor versus surrounding infiltrated brain tissue at the tumor edges are difficult to separate. ^{18}F-FGln-avidity, despite showing lower absolute SUV tumor values was minimal in the surrounding brain enabling better tumor delination.

Table S3

Area	1 hour		2 hours	
	SUV Average	Stdev	SUV Average	Stdev
Brain	0.4	0.1	0.5	0.2
Lung	0.6	0.1	0.4	0.1
Appendicular skeleton (humerus)	0.8	0.2	0.9	0.2
Skeletal muscle	1	0.1	1	0.1
Proximal aorta (blood pool)	1.3	0.2	1	0.3
Spleen	1.4	0.3	0.9	0.2
Kidney	1.7	0.5	1.2	0.5
Parotid gland	2.1	0.5	1.6	0.6
Submandibular gland	2	0.5	2.1	0.6
Small Intestine	1.8	0.5	1.4	0.3
Cardiac muscle	2	0.4	1.9	0.4
Liver	2.8	1	1.6	0.8
Axial skeleton (vertebra)	3	0.6	4.3	0.7
Pancreas	3.1	0.7	1.7	0.6

Table S3. Biodistribution of ^{18}F-FGln in human subjects.

The organ tracer uptakes are expressed as SUV (standard uptake value) average (SUV average) values. The SUV parameter is “g/mL”. Soft tissue ^{18}F-FGln uptake was highest in the pancreas, followed by liver, then myocardium, with tracer-concentrations greater than aortic blood pool activity at all time-points. Pancreas and liver demonstrated progressive tracer-clearance after the 1st hour, whereas myocardial uptake appeared constant. Brain demonstrated less activity than aortic blood pool. Soft tissue tracer concentrations in other organs were less than or equal to blood pool activity.

^{18}F-FGln activity was high in the axial skeleton and bony pelvic girdle (Figure S13), with progressive accumulation to the last imaging time-point, 2-3 hours post-injection. In contrast, tracer accumulation in the long bones of the

extremities was low, less than surrounding musculature at all time points and did not progressively accumulate. The differential skeletal accumulation in axial versus appendicular skeleton could partially represent progressive uptake of ^{18}F-FGln in the hematopoietic red marrow of the axial skeleton, red marrow typically being relatively absent in the adult appendicular skeleton, apart from bony pelvis.

Table S4

	1 minute		30 minutes		60 minutes	
	Average %	Stdev	Average %	Stdev	Average %	Stdev
^{18}F (peak 1)	20.4	12.8	16.7	15.5	35.2	20.9
^{18}F-FGln (peak 2)	73.4	17.0	79.7	14.9	62.5	17.1
^{18}F-FGlu (peak 3)	6.2	8.7	3.7	0.5	2.3	4.0

Table S4.^{18}F-FGln parent compound and radiometabolites in plasma at 1, 30, and 60 minutes after tracer injection.

Amounts expressed as percentage of sum of total activity of three identified radioHPLC peaks in each sample. Parent ^{18}F-FGln and metabolites were separated by radioHPLC, identified by characteristic radioHPLC activity peaks. The amount of each radioHPLC eluted peak was quantified by scintillation well-counting, correcting for background activity and physical decay. Amounts expressed as percentage of sum of total activity of three identified radioHPLC peaks in each sample. The 30 and 60 minute time points represent 2 and 3 patients as blood samples were either insufficient for radioHPLC or samples suffered technical artifact. RadioHPLC demonstrated the presence of free fluorine-^{18} contributing to skeletal activity. Free fluorine-^{18} measurements obtained in patients at the earliest time point (1 min post-injection) are possibly

overestimated due to the sensitivity of low count statistics to noise artifact. Radiochemical purity testing prior to ^{18}F-FGln injection confirmed the absence of free fluorine-^{18}.

Table S5

Organ	Average (rem/mCi)	Stdev
Adrenals	0.03	0.01
Brain	0.02	0.00
Breasts	0.01	0.00
Gallbladder Wall	0.04	0.01
LLI Wall	0.07	0.02
Small Intestine	0.13	0.04
Stomach Wall	0.02	0.01
ULI Wall	0.14	0.05
Heart Wall	0.05	0.02
Kidneys	0.06	0.02
Liver	0.08	0.01
Lungs	0.02	0.01
Muscle	0.04	0.01
Ovaries	0.05	0.02
Pancreas	0.09	0.01
Red Marrow	0.07	0.02
Osteogenic Cells	0.08	0.03
Skin	0.01	0.00
Spleen	0.05	0.02
Testes	0.02	0.01
Thymus	0.02	0.01
Thyroid	0.02	0.01
Urinary Bladder Wall	0.69	0.36
Uterus	0.06	0.03
Total Body	0.03	0.01
Effective Dose	0.07	0.02

Table S5. ^{18}F-FGln dosimetry in human subjects.

^{18}F-FGln radiation dosimetry in human subjects, including organ absorbed doses (rem/mCi) and effective dose (rem/mCi). For each organ, the time-activity data from the human PET-based biodistribution studies of ^{18}F-FGln were fit to an exponential function using least-squares regression (Excel, Microsoft Corp, Redmond, WA). The fitted time-activity concentration functions were analytically integrated (incorporating the effect of the physical decay of ^{18}F) and converted from concentrations to total-organ values using the 70-kg Standard Man organ masses to yield the respective organ residence times (h). The rest-of-body residence time was calculated as the difference between the total-body residence time and the sum of the normal-organ residence times. The red marrow cumulated activity was estimated from the blood residence time, assuming instantaneous equilibration of the ^{18}F activity between plasma and marrow extracellular space, a plasmacrit of 0.6, and a marrow fractional extracellular space of 0.4. Finally, the mean normal-organ radiation doses (cGy/MBq ^{18}F-FGln administered) and the effective dose (cSv/MBq [^{18}F]-fluoroglutamine administered) were calculated for the 70-kg Standard Man anatomic model with scaling of the organ masses to those of the respective patient's total-body mass using the "MIRD formalism", as implemented in the OLINDA EXM program.